Light-assisted decomposition of dyes over iron-bearing soil clays in the presence of H_2O_2

Zhaohui Wang, Wanhong Ma, Chuncheng Chen, Jincai Zhao*

Beijing National Laboratory for Molecular Sciences, Key Laboratory of Photochemistry, Institute of Chemistry, The Chinese Academy of Sciences, Beijing 100190, China

ARTICLE INFO

ABSTRACT

Four types of soil clays from different sites in China have been chosen to simulate chemical remediation of soils contaminated with dyes by light-assisted Fenton-like method. X-Ray diffraction (XRD), X-ray photoelectron spectroscopic (XPS) and electron spin resonance (ESR) measurements indicated that these soil clays contain iron oxides such as magnetite and hematite, where nondistorted iron active sites (ESR spectra, $g = 2.3$) predominate. Upon visible or UV irradiation, the soil clays were very effective for the degradation of nonbiodegradable cationic dyes such as Rhodamine B (RhB) by activating H_2O_2 at neutral pH. The photodegradation rates of RhB were closely related to total Fe content in clays and H_2O_2 dosage, indicating the mineral-catalyzed Fenton-like reactions operated. Soil organic matters (SOM) would remarkably inhibit the photodecomposition of RhB dye. The reaction products were some low-molecular-weight dicarboxylic acids and their derivatives, all of which are easily biodegradable. A possible mechanism was proposed based on the results obtained by spin-trapping ESR technique.
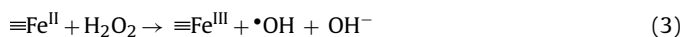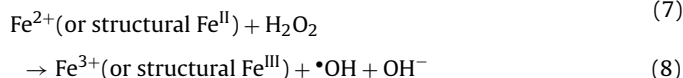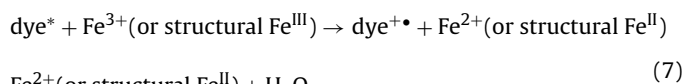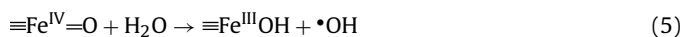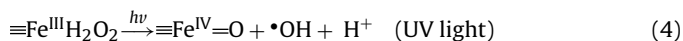
1. Introduction

Dyes are used widely in textile, plastic, dyeing, paper, printing, pharmaceutical and cosmetic industries. There are over 10,000 commercially available dyes and more than 7×10^5 tons of dyestuffs are produced annually [1]. Dyestuffs wastewater discharged from industries can contaminate the surface and the subsurface, such as soils and sediments, thus posing a severe environmental problem. At present, owing to wide usage of industrial dyes in China, the water and soil have been contaminated widely [2].

In general, the dyes used by industries have good stability, most of which are recalcitrant to light, oxidation and aerobic digestion. Bioremediation techniques have been developed to decolorize synthetic dyes, but these biological treatments have limited application due to its low efficiency especially under cold climate conditions in most areas of northern China. Also, some dyes are not subject to biological degradation because of their complicated structures and toxicity. *In situ* and on-site chemical remediation processes have an advantage over biological treatment on these aspects. Especially, Fenton' regent has successfully applied to treat soils contaminated with hazardous chemicals [3–8]. Clays in soil matrix are composed of particles less than 2 mm. Natural soil clays contain many kinds of iron oxyhydroxide minerals such as hematite, goethite

and magnetite [9], which are important competents for initiating mineral-catalyzed Fenton-like reactions when H_2O_2 is present [4].

$$\equiv Fe^{III} + H_2O_2 \leftrightarrow \equiv Fe^{III}H_2O_2 \tag{1}$$

$$\equiv Fe^{III}H_2O_2 \rightarrow \equiv Fe^{II} + HO_2^\bullet + H^+ \tag{2}$$

$$\equiv Fe^{II} + H_2O_2 \rightarrow \equiv Fe^{III} + {}^\bullet OH + OH^- \tag{3}$$

During the past decade, such a Fenton-like soil remediation has been used to treat pentachlorophenol (PCP), trichloroethylene (TCE), quinoline and other biorefractory chemicals [3,5]. However, previous investigations suggest the reduction of $\equiv Fe^{III}$ to $\equiv Fe^{II}$ (Eq. (2)) is the rate-limiting step in the overall Fenton-like reactions and thus determines the generation rate of oxidizing species—hydroxyl radical [4]. Our former work indicated that UV [10] (Eq. (4)–(5)) or visible light irradiation [11,12] (Eq. (6)–(8)) could greatly facilitate the $^\bullet OH$ generation through different ways.

$$\equiv Fe^{III}H_2O_2 \xrightarrow{h\nu} \equiv Fe^{IV}=O + {}^\bullet OH + H^+ \quad (UV \text{ light}) \tag{4}$$

$$\equiv Fe^{IV}=O + H_2O \rightarrow \equiv Fe^{III}OH + {}^\bullet OH \tag{5}$$

$$dye \xrightarrow{h\nu} dye^* \quad (visible \text{ light}) \tag{6}$$

$$dye^* + Fe^{3+}(or \text{ structural } Fe^{III}) \rightarrow dye^{+\bullet} + Fe^{2+}(or \text{ structural } Fe^{II}) \tag{7}$$

$$Fe^{2+}(or \text{ structural } Fe^{II}) + H_2O_2$$
$$\rightarrow Fe^{3+}(or \text{ structural } Fe^{III}) + {}^\bullet OH + OH^- \tag{8}$$

* Corresponding author. Tel.: +86 10 8261 0080; fax: +86 10 8261 6495.
  E-mail address: jczhao@iccas.ac.cn (J. Zhao).
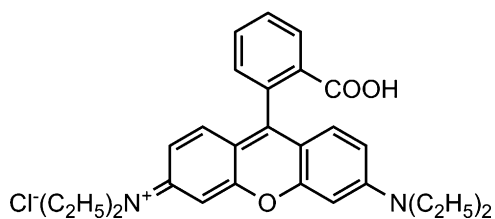
Scheme 1. Chemical structure of RhB.

Considering the fact that iron species are the most ubiquitous and chemically reactive components in soils, we hypothesized that, upon light irradiation, these Fenton-like reactions would accelerate significantly the degradation of dye pollutants in the presence of H_2O_2. Hence, the objective of this study was to examine the possible roles of iron species in soils from different sites in China in the photodegradation of dyes by Fenton-like reactions, explore and optimize the conditions that influence the photo-assisted chemical treatment of soils contaminated with industrial colorants. Rhodamine B, a common dye used in industrial case and laboratory study, was selected as target pollutant because its photodecomposition process has been extensively characterized in the previous study [13,14]. It was found that RhB could be photodegraded efficiently over the soil clays by activating H_2O_2 at neutral pH. The present investigation may provide a practical and costs-effective way using natural iron-bearing soil clays for remediation of soils contaminated with industrial dyes.

2. Experimental

2.1. Chemicals

Rhodamine B (RhB), ascorbic acid, anhydrous pyridine, 1, 10-phenanthroline, hydrogen peroxide (30% aqueous solution) were of laboratory reagent grade and used without further purification. The molecular structures of RhB are shown in Scheme 1. The spin-trapping regent 5,5-dimethyl-1-pyroline-*N*-oxide (DMPO) was purchased from Sigma Chemical Co. 1,1,1,3,3,3-hexamethyldisilazane (98%) and chlorotrimethylsilane (98%) were obtained from Acros Organics. Barnstead UltraPure water (18.3 MΩ) was used throughout the study. The initial pH was adjusted with diluted aqueous solutions of NaOH or $HClO_4$.

2.2. Soil clays

Four soil samples were collected from surface horizon (0–20 cm) at typical agricultural fields in Shenyang, Linchuan, Zhenjiang and Kaifeng in China, coded as LN, JX, JS and HN, respectively. They were air-dried, lightly ground, sieved (<2 mm) and stored in closed plastic bags at room temperature. Selected characteristics of the soils are presented in Table 1. The organic carbon content of each soil sample was determined according to the method described

by Walkey and Black [15]. The clay fraction (< 2 μm) of each soil sample was separated by the sedimentation method. Then it was flocculated with $MgCl_2$ (1 M, pH 7.0) for 2 h to remove the dissolved metal ions, washed twice with deionized water and freeze-dried. Subsequently, the clay fraction was treated with NaAc/HAc buffer (1 M, pH 4.5) to remove carbonates. Thereafter all the clay samples were treated four times with NaClO (6%, pH 9.0) for 1 h in a water bath at 85 °C to remove organic matters. After these treatments, the samples were washed (5 × 50 mL) with deionized water, and concentrated by using a rotary evaporator and then freeze-dried.

2.3. Photoreactor and light sources

The visible light source was a 500 W halogen lamp (Institute of Electric Light Source, Beijing) fixed inside a cylindrical Pyrex jacket and cooled by circulating water. A cutoff filter was positioned outside the water jacket to ensure complete visible light irradiation ($\lambda > 450$ nm). The instrumental sketch was provided elsewhere [16]. The average light luminance was determined to be 6.5×10^4 lux by digital luminometer. The UV light irradiation was from a 100 W Hg lamp ($\lambda > 330$ nm, Toshiba SHL-100UVQ-2). The light intensity for 50 mL of the solution was 1.9×10^{-7} Einstein s^{-1}.

2.4. Procedures and analysis

Unless otherwise specified, all irradiation experiments were performed in a cylindrical Pyrex vessel (70 mL) at an initial pH of 7.0. The degradation of RhB was carried out after an overnight stirring in the dark to ensure the adsorption/desorption equilibrium between dye and soil clays. At given reaction time intervals, samples (2 mL) were withdrawn, centrifuged and immediately analyzed on a Hitachi U-3100 UV–vis spectrophotometer. GC–MS data were obtained on a Trio-2000 apparatus (Micromass, UK, Ltd.) equipped with a BPX70 column (size 30 mm × 0.25 mm). The samples after 12 h of irradiation were filtered, and the filtrate was then concentrated by a rotary evaporator and freeze-dried overnight. The residue was finally redissolved in 200 μL anhydrous pyridine, followed by the addition of 100 μL hexamethyldisilazane and 50 μL of chlorotrimethylsilane [17]. The silylated sample was further analyzed by GC–MS.

X-Ray diffraction (XRD) patterns were recorded on a Philips MPD 18801 X-ray diffractometer equipped with Cu Kα radiation. X-Ray photoelectron spectroscopic (XPS) measurement of the samples was carried out on the 2201-XL multifunctional spectrometer (VG Scientific England) using Al Kα radiation. Electron spin resonance (ESR) spectra of radicals spin-trapping by DMPO were recorded at room temperature on a Bruker EPR ELEXSYS 500 spectrometer equipped with an *in situ* irradiation source (a Quanta-Ray ND:YAG laser system $\lambda = 532$ nm). For the measurement of solid samples, The ESR signals were registered at microwave power 6.364 mW and modulation amplitude 1.0 G in the field range of 480–6000 G. OriginPro 7.5 (OriginLab Corporation, USA) was used to fit the experimental data and simulate the three Lorentzian components.

Table 1
Selected metal content and characteristics of the original soil samples.

Samples	Trace metal content[a] (g kg^{-1})		Clays properties			
	Fe	Ti	pH[b] (1:2.5)	ρ (g cm^{-3})	w (H$_2$O) (g kg^{-1})	O.M.[c] (g kg^{-1})
JX	36.7	5.1	5.1	2.10	30.4	5.7
HN	24.9	3.7	8.1	1.86	27.5	12.1
JS	41.2	5.6	5.4	2.16	53.5	26.6
LN	23.9	4.6	5.5	2.25	43.6	31.8

[a] Measured by inductively coupling plasma-atomic emission spectra (ICP-AES).
[b] Soil/water ratio (g mL^{-1}) = 1:2.5.
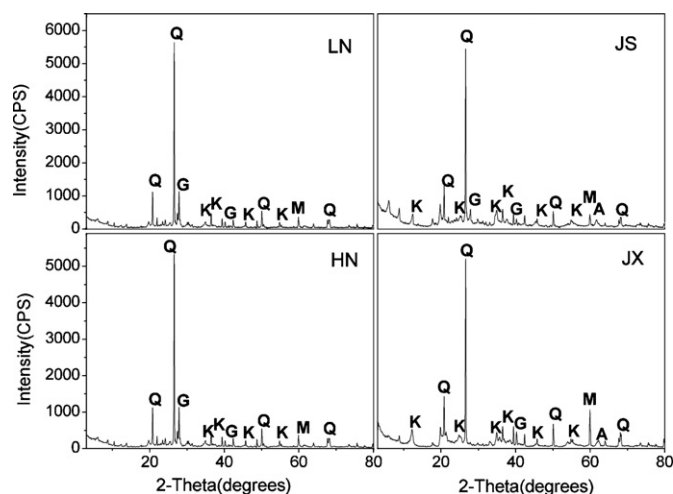[c] Organic matters.

Fig. 1. X-Ray diffractograms of original soil samples. Q, quartz; K, kaolinite; G, gibbsite; A, anatase; M, magnetite. Rutile and hematite were not marked for clarity.

3. Results and discussion

3.1. Characterization of the soil clays

The XRD patterns of the four original soil samples are shown in Fig. 1. XRD data were collected in the angular range (3–80°). All soil samples showed very similar patterns. The soils mainly consist of quartz, kaolinite and gibbsite, with trace iron oxide (i.e. magnetite and hematite) and titanium oxide like anatase and rutile [18,19]. Nevertheless, not all their characteristic peaks for Fe and Ti oxides were identified possibly due to the interference and coverage with abundant Al and Si oxides.

For better understanding the property of the iron oxides in the original soils, XPS analysis is used to survey the chemical states of the iron species. The XPS spectra of Fe 2p for the soil clays are shown in Fig. 2. The broad Fe $2p_{3/2}$ spectra present a major contribution occurring at near 712.5 eV, which corresponds to the binding energy of Fe(III)–O. The difference between Fe $2p_{3/2}$ and Fe $2p_{1/2}$ peaks, 13.7 eV, is slightly higher than that found for Fe_2O_3 (13.6 eV) [20]. This result is consistent with the XRD patterns, which shows the occurrence of some iron oxides.

Fig. 3 shows the ESR spectrum for the JX sample, which was similar to those recorded from other soil samples (data not shown). It was reported that different g factors, i.e. 4.2, 2.3 and 2.0 were
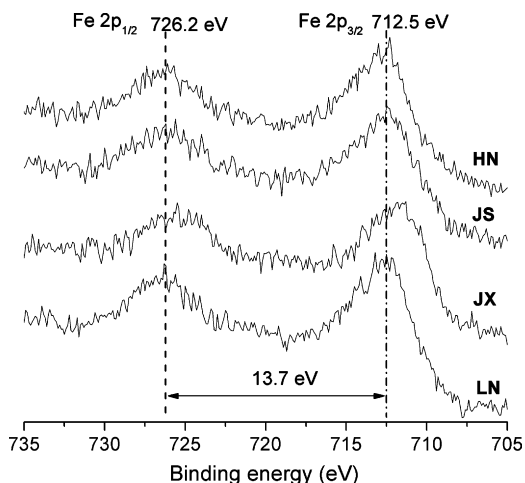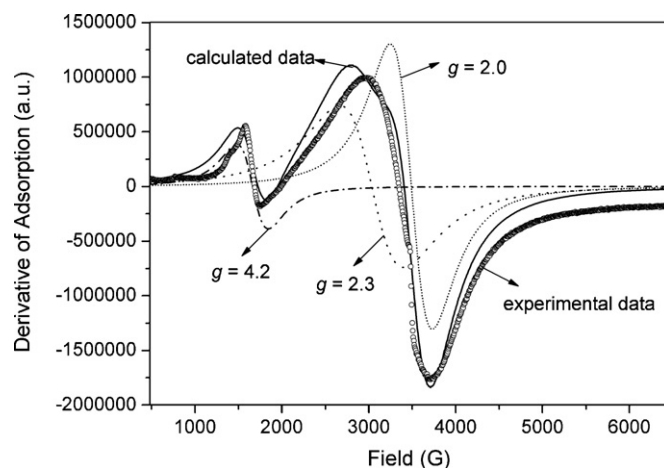

Fig. 3. X-Band ESR spectrum of JX sample. The open circles represent the experimental data, the solid line is the best fit and dashed lines are the Lorentzian components.

assigned to be representative of cubic distorted sites (occupying silicon tetrahedral framework positions), nondistorted sites (occupying oxy or hydroxyl species interstitial positions) and separate ferric oxide phases, respectively [18,21,22]. The experimental data could be fitted to three Lorentzian curves corresponding to the three different g factors (Fig. 3). The calculated ESR parameters, such as FWHM (full width at half maximum) and peak height are listed in Table 2. Although we could not calculate the each concerning Fe concentration with corresponding g factor in terms of its respective area fraction [18], it is clear that the nondistorted iron sites (g = 2.3) are predominant among the three coordination sites.

3.2. Kinetic study of RhB photodegradation

RhB degradation was carried out after the adsorption/desorption equilibrium has been achieved between dye and soil clays. RhB did not react with H_2O_2 over LN soil clay in the dark (Fig. 4, curve a), or in the absence of soil clay under visible light irradiation (curve b). Upon visible light illumination, 30% of RhB in RhB/LN soil clay dispersion was decolored after 12 h of reaction time (curve c). However, as H_2O_2 was added in this dispersion, RhB could be photodegraded much rapidly under visible irradiation (curve d). Similarly, photodegradation of RhB also was observed when other three soil clays were added. As shown in Table 1 and XRD patterns, natural soils contain some semiconductor minerals, such as titanium oxide and iron oxide, which may be involved in
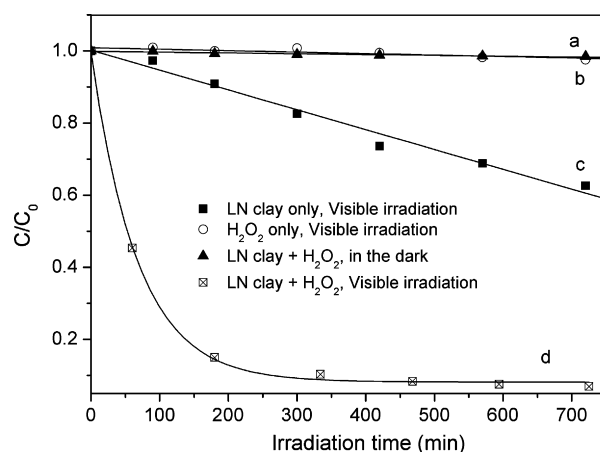

Fig. 2. XPS spectra of Fe 2p for the different soil clays.

Fig. 4. RhB photodegradation in LN soil clay dispersion under different conditions. Soil clay, 15 mg; RhB, 20 µM; H_2O_2, 4000 µM; pH, 7.0.

Table 2
ESR parameters for three components obtained from simulation as shown in Fig. 3.

	$g = 2.0$			$g = 2.3$			$g = 4.2$		
	FWHM[a]	H[b]	A[c]%	FWHM	H	A%	FWHM	H	A%
LN	358.9	5.6×10^8	24.6	639.9	1.0×10^9	73.6	318.2	4.6×10^7	1.7
JX	418.9	8.4×10^8	41.5	637.3	7.3×10^8	51.7	314.7	1.9×10^8	6.8
JS	469.6	1.1×10^8	17.5	799.4	3.3×10^8	79.0	324.2	3.3×10^7	3.5
HN	386.7	1.4×10^8	25.9	680.6	2.3×10^9	72.9	261.3	8.8×10^7	1.1

[a] FWHM, full width at half maximum.

[b] H, peak height.

[c] A, integral area, A%, area fraction for each g factor.

the dye-sensitized oxidation under visible irradiation. The excited dye molecule injects an electron into the conductor band of semiconductor, while dye itself is converted to a cationic radical. The injected electron reacts with the dioxygen adsorbed on TiO_2, thus yielding superoxide radical anions and then other active oxygen species. These primary steps for the degradation of dyes in the presence of titanium oxide under visible irradiation have been evidenced by our and other groups [23–26].

Therefore, the photoactive semiconductor minerals may act as an electron relay, thus causing the degradation of dye, even in the absence of other oxidants like H_2O_2. Nevertheless, this kind of dye-sensitized photodegradation (curve c) would be much slower comparing with the heterogeneous Fenton-like reaction (curve d).

The rate constants k (min^{-1}) for the dye degradation were calculated from linear regression $-\ln(C/C_0)$ versus time plots. It was observed that kinetics data obtained for LN and other three soil clays dispersion followed pseudo-first-order kinetics in the presence of H_2O_2, which consistent with the reported facts that the heterogeneous Fenton-like reaction for dye degradation typically follows pseudo-first-order kinetics at relatively low pollutant concentration [6–8]. It also proves that Fenton-like reaction dominated in the process of photodegradation of dye as discussed above.

All the obtained pseudo-first-order rate constants are summarized in Table 3. It was found that the addition of H_2O_2, either under UV or visible irradiation, could enhance the rates of RhB degradation for all soil clay systems, especially for the LN sample. Several investigators indicated that catalytic decomposition of hydrogen peroxide and pollutants would depend on the specific feature of the iron species. Huang et al proved that hematite exhibited the highest catalytic activity for 2-chlorophenol oxidation among goethite, hematite and granular ferrihydrite, the three widespread iron oxides in soils and sediments [27]. We reported in the previous work that goethite (α-FeOOH) could accelerate the degradation of azo dye pollutants upon the addition of H_2O_2 at neutral pHs under UV irradiation [10]. Furthermore, it is evidenced that free iron oxides in clay mineral were capable of promoting the decomposition of H_2O_2 [11]. Structural Fe(III) that substitutes aluminum in the octahedral lattice, as identified in Fig. 3 ($g = 4.2$), can also undergo Fenton-like reactions in the presence of particular photoreactive organic species (Eq. (6)–(8)) [11,12]. Therefore, we concluded that the active iron species should be responsible for catalytic oxidation of dye in the current systems. Although it is difficult to evaluate

accurately the respective contribution of three kinds of iron species for each soil clay to the dye degradation, photodegradation rates of dye largely correlated with total Fe contents in different types of soils [28]. For example, LN soil clay had two-fold total Fe content than JX, the difference in their rate constants under the same conditions was quite remarkable too. However, there was still a large difference in rate constants between LN and JS samples, although their total Fe contents were nearly equal.

3.3. Effect of soil organic matters (SOM)

Soil organic matters are mostly composed of humic substances and likely to either enhance or inhibit the rate of the photodegradation of organic contaminants. Voelker and Sulzberger found that fulvic acid may enhance the rates for Fenton reaction by complexing with Fe^{2+} [29]. In contrast, Tyre et al. reported that pentachlorophenol exhibited low oxidation efficiency in soils of high organic content whereas the Fenton oxidation of hexadecane seemed not susceptible to SOM [5]. In our study, similar inhibitory effect of SOM on the RhB photodegradation was observed in Fig. 5, namely, LN-Org soil clay (without removal of organic matters) had a lower reaction rate than the treated soil clay under both UV and visible irradiation.

Several reasons may account for this kind of inhibitory effect caused by soil organic matters: (i) energy transfer and charge transfer between the dye and SOM can deactivate the excited dye molecule; (ii) the active iron oxide species of soils are likely to be enveloped by organic matters, thus inhibiting the interaction among these species, dye molecule and H_2O_2; (iii) SOM consumes and competes for reactive oxidants generated from Fenton reaction [30]. In addition, SOM inhibits remarkably the adsorption of dye on soil clays as shown in Fig. 5. The preliminary adsorption of dye has
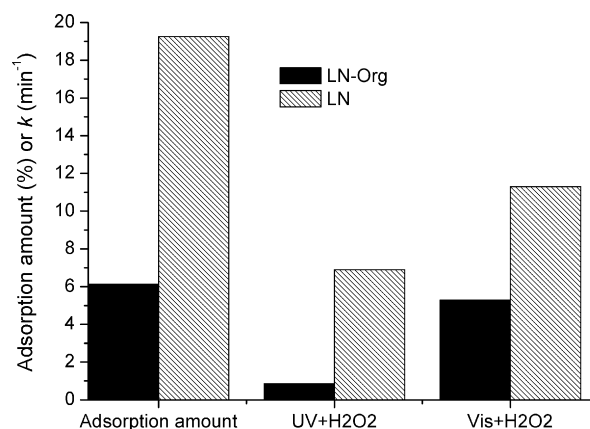
Table 3
Comparisons of the Fe content of extracted soil clays and pseudo-first-order rate constant of RhB photodegradation under various conditions.

Clay	Fe content $(g\,kg^{-1})$	Pseudo-first-order rate constant k $(10^{-4}\,min^{-1})$	
		$UV + H_2O_2$	$Vis + H_2O_2$
LN	43.5	6.9	11.3
JS	41.1	2.7	4.3
HN	40.9	4.8	4.2
JX	23.6	2.5	1.9

Conditions: soil clay, 15 mg; RhB, 20 μM; H_2O_2, 10 μM; pH 7.0.

Fig. 5. Effects of SOM on adsorption and degradation rate of dye over LN soil clay under UV or visible light irradiation. Adsorption amount was obtained from the difference between the concentrations of dye before and after 30 min of adsorption/desorption equilibrium. LN-Org denotes LN soil clay without removal of organic matters. Soil clays, 15 mg; RhB, 20 μM; H_2O_2, 10 μM; pH, 7.0.
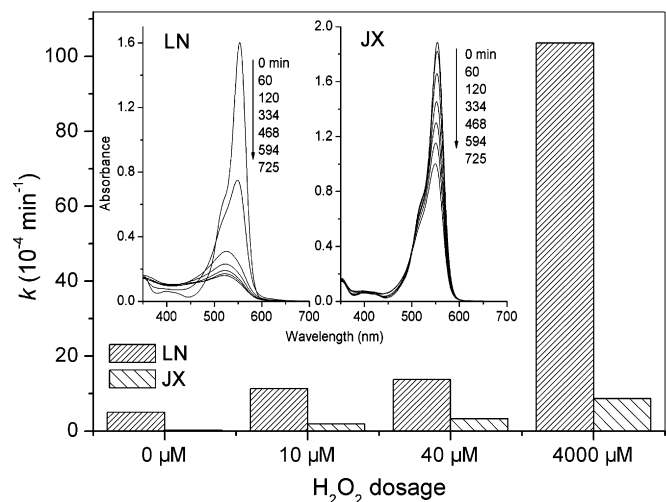
Fig. 6. Effect of H_2O_2 dosage on the photodegradation of RhB in soil clays dispersion under visible light irradiation. *Inset*: UV–vis spectral changes of RhB in soil clays/H_2O_2 (4000 μM) dispersion under visible light irradiation. Soil clays, 15 mg; RhB, 20 μM; pH, 7.0.

been verified as an important factor influencing photodegradation efficiency.

3.4. Effect of H_2O_2 dosage

The photodegradation of RhB was performed at different H_2O_2 concentrations. The degradation rate of RhB obviously increased as H_2O_2 dosage increased as expected. For LN soil clay, the rate constant for the photodegradation of dye increased by a factor of 10 as the H_2O_2 concentration increased from 10 to 4000 μM. The temporal UV–vis spectra (inset plot in Fig. 6) show that RhB characteristic band centered at 533 nm was rapidly declined upon visible irradiation, concomitantly with a blue shift at the maximum absorption, which has been previously attributed to the destroy of the chromophoric structure concomitantly with the *N*-de-ethylation of RhB during the degradation process [12,31]. As compared to LN sample, JX soil clay was not susceptible to H_2O_2 dosage: much more H_2O_2 failed to accelerate the dye degradation under the otherwise identical conditions. Higher concentration of H_2O_2 may scavenge parts of reactive oxidative species like •OH radical (Eq. (9)), thus decreasing the degradation efficiency of dye pollutant. The UV–vis spectra for
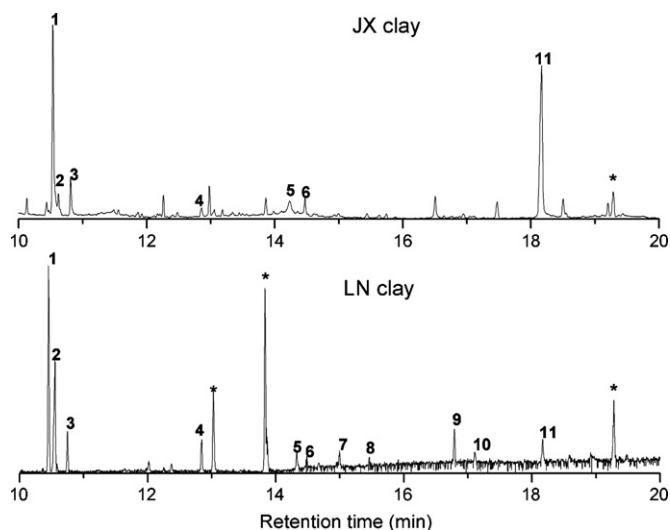

Fig. 7. GC chromatograms of the samples obtained from the RhB photodegradation in soil clays/H_2O_2 dispersion after 12 h of visible light irradiation. The asterisk (*) denotes the unidentified products. Soil clays, 15 mg; RhB, 20 μM; H_2O_2, 4000 μM; pH, 7.0.

the JX sample displayed a slow decrease of the characteristic peak at 533 nm, where no blue shift was observed. This result implies that the H_2O_2 concentration is a rate-determining factor in soil remediation and reaction efficiency is highly dependent of the nature of soils.

$$\bullet OH + H_2O_2 \rightarrow H_2O + HO_2\bullet \tag{9}$$

3.5. Intermediates identification

The reaction products and intermediates of RhB during the photodegradation in LN and JX systems were measured by GC–MS technique. The GC chromatograms and identified intermediates are shown in Fig. 7 and Table 4, respectively. The main intermediates were low-molecule-weight dicarboxylic acids and their hydroxylated derivatives. Some aromatic compounds like salicylic acid, phthalic acid and its ester derivatives were also detected. Small molecular compounds such as HCOOH, $HCON(CH_3)_2$ and $HCONHCH_3$ were not detected because they were easily evaporated during the sample preparation. The present result, together with
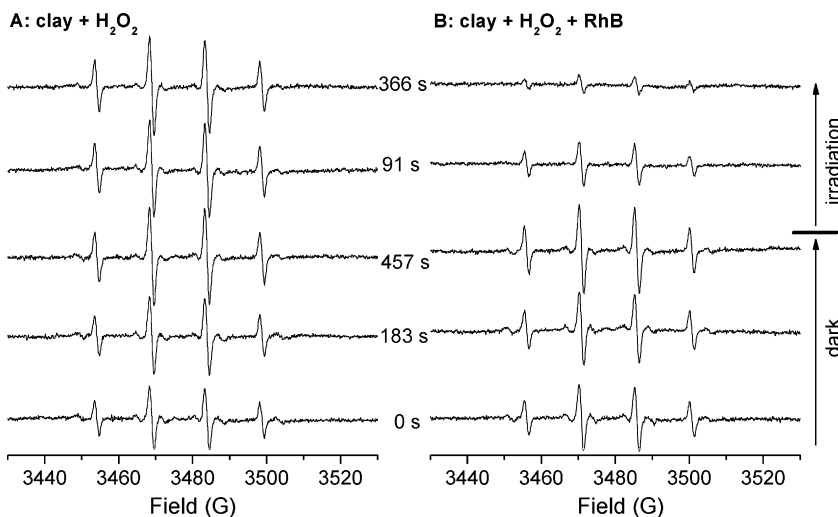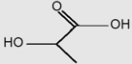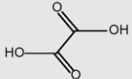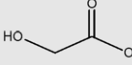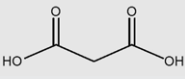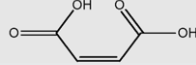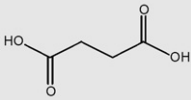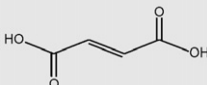

Fig. 8. ESR spectra for the systems of (A) clay + H_2O_2 and (B) clay + H_2O_2 + RhB in the dark and under 532 nm laser irradiation. DMPO, 0.04 M; LN clay, 50 mg; RhB, 20 μM; H_2O_2, 6 mM; pH 7.0.

Table 4
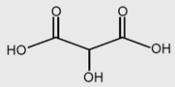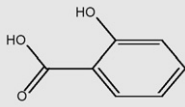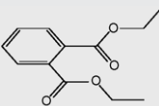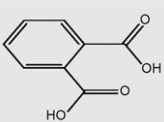Retention times and the identified products corresponding to Fig. 7.

Peak no.	R.T. (min)	Products	Structural formula
1	10.45	Lactic acid	
2	10.55	Oxalic acid	
3	10.75	Glycolic acid	
4	12.84	Malonic acid	
5	14.33	Maleic acid	
6	14.49	Succinic acid	
7	14.99	Fumaric acid	
8	15.47	2-Hydroxymalonic acid	
9	17.11	Salicylic acid	
10	18.17	Diethyl phthalate	
11	19.28	Phthalic acid	

has proved a more effective catalyst in Fenton-like reaction as compared to other iron oxides, because Fe^{2+} in its structure facilitates the production of $^{\bullet}OH$. Therefore, the DMPO–$^{\bullet}OH$ signal could be readily observed and temporally evolved even in the dark.

An interesting behavior in ESR signal evolution was observed when samples were exposed to laser irradiation: DMPO–$^{\bullet}OH$ signal rapidly decayed in the presence of RhB (Fig. 8B) whereas the intensity of the four-fold peak continued to increase without addition of dye (Fig. 8A). The quick decay of DMPO–$^{\bullet}OH$ adducts, similarly observed in the other clays (data not shown), may result from: (i) quenching by Fe^{2+} if $[Fe^{2+}] \gg [H_2O_2]$ [32]; (ii) competitive reaction with $^{\bullet}OH$ between dye and spin-trapping regent DMPO; (iii) oxidation of DMPO–$^{\bullet}OH$ adducts by active oxidants like ferryl (Fe^{IV}=O) [33]. (i) is not feasible because we used $[H_2O_2]:[Fe^{2+}] > 7.7$ (assuming all iron existed in soil is ferrous state) in ESR experiments. Also, (ii) seems also impossible due to the fact that DMPO–$^{\bullet}OH$ signal always increased in the dark, even in the presence of dye (Fig. 8B), indicating RhB itself does not apparently inhibit the production of DMPO–OH adducts. We also eliminated the possibility of rapid quenching of the DMPO–OH by the excited dye molecule due to the fact that DMPO–$^{\bullet}OH$ signal rose continuously in the irradiated RhB/H_2O_2 system in the presence of ferrous ions loaded on laponite (a synthetic magnesiansilicate clay) [12]. Therefore, we wish to accept the third interpretation. Formation of the ferryl ion (FeO^{2+}-chelate) might be favored at neutral pH values [34]. High valent iron-oxo species have been ever proposed in H_2O_2-dependent redox chemistry of iron–EDTA complex [35]. Hasinoff also postulated that high valence iron-oxo species might be responsible for the degradation of calcein at pH 7.4 [36]. Recently, a non-heme Fe(IV)=O complex has been structurally and spectroscopically characterized by Que and co-workers [37].

In the present work, RhB may anchor on the surface of iron oxides through its carboxylic moiety (–COOH) [31], thus facilitating the electron transfer between RhB and iron species. Once upon visible irradiation, excited dye molecule can donor electrons to ≡Fe^{III}, which is therefore reduced to ferrous state. The newly generated ≡Fe^{II} react with H_2O_2 in the presence of dye to yield a ≡FeO^{2+}–dye intermediate instead of $^{\bullet}OH$. The high valent species Fe(IV)=O also have high oxidative activity, and can degrade the adjacent RhB molecules to yield some organic acids. However, Since Fe(IV)=O is such a highly reactive and transient intermediate, it was difficult to detect directly under our experimental conditions. Further study is needed for detailed reaction mechanism.

4. Conclusions

Iron oxide species in four soils have been identified by XRD, XPS and ESR techniques, which were proved to be responsible for mineral-catalyzed Fenton-like reactions. Upon visible and UV irradiation, the soil clays in the presence of H_2O_2 were effective for the degradation of nonbiodegradable cationic dye – Rhodamine B (RhB) by Fenton-like reaction at neutral pH. Soil organic matters had adverse effect on the dye photodegradation. The reaction products identified by GC–MS were some low-molecular-weight dicarboxylic acids and their derivatives, both of which are easily degraded by bioremediation. The present study proved the feasibility for in-situ photochemical remediation of soils contaminated with industrial colorants.

UV–vis spectra, suggests that the RhB photodegradation should simultaneously proceed through cleavage of chromophore ring structure and N-de-ethylation.

3.6. Reactive oxygen species assays

Spin-trapping ESR technique was employed to identify the possible short-lived reactive oxygen species involved in the reaction mechanism. For this study, all the ESR spectra were recorded by in situ laser irradiation (532 nm) using DMPO as the radical trapping agent. Whether the dye substrate was added or not, a four-fold characteristic peak of DMPO–$^{\bullet}OH$ adducts with an intensity ratio of 1:2:2:1 [11], was observed when soil clay and H_2O_2 were mixed in the dark (Fig. 8). As identified in the XRD results, ferric oxide including magnetite and hematite existed in all the four soils. Magnetite

Pollution Control and Resource Reuse, School of the Environment, Nanjing University) for his kindly providing soil samples.

References

[1] H. Zollinger, Colour Chemistry-Synthesis, Properties and Applications of Organic Dyes and Pigments, VCH Publishers, New York, 1987.

[2] Q.X. Zhou, Chemical pollution and transport of organic dyes in water-soil-crop systems of the Chinese coast, Bull. Environ. Contam. Toxicol. 66 (2001) (2001) 784–793.

[3] S.-H. Kong, R.J. Watts, J.-H. Choi, Treatment of petroleum-contaminated soils using iron mineral catalyzed hydrogen peroxide, Chemosphere 37 (1998) 1473–1482.

[4] W.P. Kwan, B.M. Voelker, Rates of hydroxyl radical generation and organic compound oxidation in mineral-catalyzed Fenton-like systems, Environ. Sci. Technol. 37 (2003) 1150–1158.

[5] B.W. Tyre, R.J. Watts, G.C. Miller, Treatment of four biorefractory contaminants in soils using catalyzed hydrogen peroxide, J. Environ. Qual. 20 (1991) 832–838.

[6] K. Dutta, S. Bhattacharjee, B. Chaudhuri, S. Mukhopadhyay, Chemical oxidation of CI Reactive Red 2 using Fenton-like reactions, J. Environ. Monit. 4 (2002) 754–760.

[7] M. Neamtu, A. Yediler, I. Siminiceanu, A. Kettrup, Oxidation of commercial reactive azo dye aqueous solutions by the photo-Fenton and Fenton-like process, J. Photochem. Photobiol. A: Chem. 161 (2003) 87–93.

[8] K. Hanna, T. Kone, G. Medjahdi, Synthesis of mixed oxides of iron and quartz and their catalytic activities for the Fenton-like oxidation, Catal. Commun. 9 (2008) 955–959.

[9] U. Schwertmann, R.M. Cornell, Iron Oxide in the Laboratory: Preparation and Characterization, VCH Publishers, New York, 1991.

[10] J. He, W. Ma, J. He, J. Zhao, J.C. Yu, Photooxidation of azo dye in aqueous dispersions of H_2O_2/α-FeOOH, Appl. Catal. B: Environ. 39 (2002) 211–220.

[11] W. Song, M. Cheng, J. Ma, W. Ma, C. Chen, J. Zhao, Decomposition of hydrogen peroxide driven by photochemical cycling of iron species in clay, Environ. Sci. Technol. 40 (2006) 4782–4787.

[12] M. Cheng, W. Song, W. Ma, C. Chen, J. Zhao, J. Lin, H. Zhu, Catalytic activity of iron species in layered clays for photodegradation of organic dyes under visible irradiation, Appl. Catal B: Environ. 77 (2008) 355–363.

[13] W. Ma, J. Li, X. Tao, J. He, Y. Xu, J.C. Yu, J. Zhao, Efficient degradation of organic pollutants by using dioxygen activated by resin-exchanged iron(II) bipyridine under visible irradiation, Angew. Chem. Int. Ed. 42 (2003) 1029–1032.

[14] M. Cheng, W. Ma, C. Chen, J. Yao, J. Zhao, Photocatalytic degradation of organic pollutants catalyzed by layered iron(II) bipyridine complex-clay hybrid under visible irradiation, Appl. Catal B: Environ. 65 (2006) 217–226.

[15] Walkey, I.A. Black, An examination of the Degtjareff method for determining soil organic matter and proposed modification of the chromic acid titration method, Soil Sci. 37 (1934) 29–38.

[16] M. Cheng, W. Ma, J. Li, Y. Huang, J. Zhao, Visible-light-assisted degradation of dye pollutants over Fe(III)-loaded resin in the presence of H_2O_2 at neutral pH values, Environ. Sci. Technol. 38 (2004) 1569–1575.

[17] C. Sweeley, R. Bentley, M. Makita, W.W. Wells, Gas-liquid chromatography of trimethylsilyl derivatives of sugars and related substances, J. Am. Chem. Soc. 85 (1963) 2497–2507.

[18] R.S.T. Manhães, L.T. Auler, M.S. Sthel, J. Alexandre, M.S.O. Massunaga, J.G. Carrió, D.R. dos Santos, E.C. da Silva, A. Garcia-Quiroz, H. Vargas, Soil characterisation using X-ray diffraction, photoacoustic spectroscopy and electron paramagnetic resonance, Appl. Clay Sci. 21 (2002) 303–311.

[19] R.M. Torres Sánchez, M. Okumura, R.C. Mercader, Charge properties of red Argentine soils as an indicator of iron oxide/clay associations, Aust. J. Soil Res. 39 (2001) 423–434.

[20] C.D. Wagner, W.M. Riggs, L.E. Davis, J.F. Moulder, Handbook of X-Ray Photoelectron Spectroscopy: a Reference Book of Standard Data for Use in X-Ray Photoelectron Spectroscopy, Perkin-Elmer Corporation, Eden Prairie, Minn, 1979.

[21] B. Sutter, T. Wasowicz, T. Howard, L.R. Hossner, D.W. Ming, Characterization of iron, manganese, and copper synthetic hydroxyapatites by electron paramagnetic resonance spectroscopy, Soil Sci. Soc. Am. J. 66 (2002) 1359–1366.

[22] D. Coldfarb, M. Bemardo, K.G. Strohmaier, D.E.W. Vaughan, H. Tbomann, Characterization of iron in zeolites by X-band and Q-band ESR, Pulsed ESR, and UV-visible spectroscopies, J. Am. Chem. Soc. 116 (1994) 6344–6353.

[23] F.L. Zhang, J.C. Zhao, T. Shen, H. Hidaka, E. Pelizzetti, N. Serpone, TiO_2-assisted photodegradation of dye pollutants. II. Adsorption and degradation kinetics of eosin in TiO_2 dispersions under visible light irradiation, Appl. Catal. B Environ. 15 (1998) 147–156.

[24] T.X. Wu, G.M. Liu, J.C. Zhao, H. Hidaka, N. Serpone, Photoassisted degradation of dye pollutants. V. Self-photosensitized oxidative transformation of Rhodamine B under visible light irradiation in aqueous TiO_2 dispersions, J. Phys. Chem. B 102 (1998) 5845–5851.

[25] W. Zhao, C.C. Chen, X.Z. Li, J.C. Zhao, H. Hidaka, N. Serpone, Photodegradation of sulforhodamine-B dye in platinized titania dispersions under visible light irradiation: influence of platinum as a functional co-catalyst, J. Phys. Chem. B 106 (2002) 5022–5028.

[26] H. Kyung, J. Lee, W. Choi, Simultaneous and synergistic conversion of dyes and heavy metal ions in aqueous TiO_2 suspensions under visible-light illumination, Environ. Sci. Technol. 39 (2005) 2376–2382.

[27] H.-H. Huang, M.-C. Lu, J.-N. Chen, Catalytic decomposition of hydrogen peroxide and 2-chlorophenol with iron oxides, Water Res. 35 (2001) 2291–2299.

[28] Z. Zhao, X. Quan, J. Chen, J. Niu, S. Chen, D. Xue, Y. Zhao, Photodegradation of γ-666 on soils: kinetics and the influence of soil organic matter and activated iron, Acta Sci. Circum. 22 (2002) 80–85.

[29] B. Voelker, B. Sulzberger, Effects of fulvic acid on Fe(II) oxidation by hydrogen peroxide, Environ. Sci. Technol. 30 (1996) 1106–1114.

[30] L.L. Bissey, J.L. Smith, R.J. Watts, Soil organic matter–hydrogen peroxide dynamics in the treatment of contaminated soils and groundwater using catalyzed H_2O_2 propagations (modified Fenton's reagent), Water Res. 40 (2006) 2477–2484.

[31] Q. Wang, C. Chen, D. Zhao, W. Ma, J. Zhao, Change of adsorption modes of dyes on fluorinated TiO_2 and its effect on photocatalytic degradation of dyes under visible irradiation, Langmuir 24 (2008) 7338–7345.

[32] L. Li, Y. Abe, K. Kanagawa, N. Usui, K. Imai, T. Mashino, M. Mochizuki, N. Miyata, Distinguishing the 5,5-dimethyl-1-pyrroline N-oxide (DMPO)-OH radical quenching effect from the hydroxyl radical scavenging effect in the ESR spin-trapping method, Anal. Chim. Acta 512 (2004) 121–124.

[33] D. de Bono, W.D. Yang, M.C. Symons, The effect of myoglobin on the stability of the hydroxyl-radical adducts of 5,5 dimethyl-1-pyrroline-N-oxide (DMPO), 3,3,5,5 tetramethyl-1-pyrroline-N-oxide (TMPO) and 1-alpha-phenyl-tert-butyl nitrone (PBN) in the presence of hydrogen peroxide, Free Radical Res. 20 (1994) 327–332.

[34] W.H. Koppenol, J.F. Liebman, The oxidizing nature of the hydroxyl radical. Comparison with the ferryl ion (FeO^{2+}), J. Phys. Chem. 88 (1984) 99–101.

[35] S.Y. Qian, G.R. Buettner, Iron and dioxygen chemistry is an important route to initiation of biological free radical oxidations: an electron paramagnetic resonance spin trapping study, Free Radical Biol. Med. 26 (1999) 1447–1456.

[36] B.B. Hasinoff, The intracellular iron sensor calcein is catalytically oxidatively degraded by iron(II) in a hydrogen peroxide-dependent reaction, J. Inorg. Biochem. 95 (2003) 157–164.

[37] J.U. Rohde, J.H. In, M.H. Lim, W.W. Brennessel, M.R. Bukowski, A. Stubna, E. Munck, W. Nam, L. Que Jr., Crystallographic and spectroscopic characterization of a nonheme Fe(IV)=O complex, Science 299 (2003) 1037–1039.